Electrochemical features of $LiMnPO_4$ olivine prepared by sol-gel pathway

Daniele Di Lecce[1], Tao Hu[2] and Jusef Hassoun[3*]

[1] *Sapienza University of Rome, Chemistry Department, P.le Aldo Moro 5, 00185 Rome, Italy*

[2] *University of Oulu, Research Unit of Sustainable Chemistry, P.O. Box 3000, FI-90014 Oulu, Finland*

[3] *Department of Chemical and Pharmaceutical Sciences, University of Ferrara, Via Fossato di Mortara, 17, 44121, Ferrara, Italy*

* Corresponding author: jusef.hassoun@unife.it

Keywords

$LiMnPO_4$; olivine; sol-gel; lithium diffusion; battery; impedance spectroscopy

Abstract

$LiMnPO_4$ is a potential cathode for lithium-ion battery of high thermal stability, low cost, environmental sustainability and high theoretical energy density. However, this intriguing olivine material suffers from intrinsic sluggish kinetics of lithium (de)insertion, which limits the reversible reaction in practical lithium cells. Herein we report a careful study of the impedance features of $LiMnPO_4$ during electrochemical reaction in lithium cell. The $LiMnPO_4$ material is prepared by sol-gel method and fully characterized by X-ray diffraction (XRD), thermogravimetric analysis (TGA), scanning electron microscopy (SEM), and transmission electron microscopy (TEM). The material shows suitable galvanostatic cycling with a working voltage of about 4.1 V, which is higher than the 3.5 V value expected from the most common olivine material, i.e., $LiFePO_4$, however with a low specific capacity. Hence, electrochemical impedance spectroscopy (EIS) is used to study the lithium (de-)insertion within the $LiMnPO_4$ structure. The results indicate an impedance behavior depending on the state of charge and a lithium diffusion coefficient trend slightly decreasing during

cell operation within the 10^{-14} – 10^{-13} cm^2 s^{-1} range. The electrochemical study in lithium cell reveals remarkable enhancement of the electrode kinetics at 70°C, which suggests preferred application of $LiMnPO_4$ materials at the higher temperatures.

Introduction

The use of phospho-olivine cathodes in lithium secondary batteries was firstly investigated in the late ninety with promising results [1,2]. Afterward, intense research efforts [3–6] focused on the use of $LiFePO_4$ as new positive electrode characterized by improved thermal stability [7], low cost, and modest environmental impact [8] compared to Co-based layered oxides. $LiFePO_4$ has working potential of about 3.5 V vs. Li^+/Li and theoretical capacity of 170 mAh g^{-1}, which leads to a theoretical energy density of about 600 Wh kg^{-1} [2,3]. Basing on several works reporting on its enhanced electrochemical properties, $LiFePO_4$ of various morphologies has been proposed as the positive electrode in commercial lithium-ion batteries [8,9].

The growing interest towards high-energy storage devices promoted studies of phospho-olivines based on Mn, Co, and Ni, thus characterized by increased electrochemical potential [10–16]. Among them, $LiMnPO_4$ was widely investigated due to promising electrochemical features, such as a specific capacity comparable to $LiFePO_4$ and working voltage of 4.1 V vs. Li^+/Li, which lead to a higher theoretical energy density (700 Wh kg^{-1}) with respect to $LiFePO_4$ [17]. Additional advantages of $LiMnPO_4$ are represented by its low cost, limited environmental impact, and high thermal stability with respect to conventional Co-based oxide cathodes, used in the most common lithium-ion battery configuration [18]. However, many works pointed out the intrinsic slow kinetics of $LiMnPO_4$ olivine phases [19–21], which require careful tuning of the synthetic parameters to produce electrode materials with satisfactory electrochemical performances [22–27]. $LiMnPO_4$ cathode is characterized by: *i)* electronic conductivity values lower than 10^{-9} S cm^{-1} [20,28]; *ii)* polaron (electrons and holes) migration barrier higher with respect to $LiFePO_4$, both for lithiated and delithiated phases [29]; *iii)* strong Jahn-Teller deformation of Mn^{3+} hindering the $LiMnPO_4$ delithiation and leading to $LiMnPO_4/MnPO_4$ interphase mismatch [19,21]. The lithium diffusion

coefficient (D_{Li^+}) of $LiMnPO_4$ was reported within a wide range [30–40]. In particular, variation of D_{Li^+} by changing the electrode state of charge has been reported in lithium cell using several olivine electrodes [33,35,40]. In this work we investigate a $LiMnPO_4$ prepared by sol-gel approach. The electrode is characterized by XRD, TGA, and electron microscopy. Hence, the electrochemical study in lithium cell is performed at room temperature as well as at 70°C by coupling EIS and galvanostatic cycling, in order to fully investigate the electrode kinetics.

Materials and methods

$LiMnPO_4$ was synthesized by a sol-gel method. A water solution containing lithium dihydrogen phosphate (LiH_2PO_4, Sigma-Aldrich), manganese acetate tetrahydrate ($(CH_3COO)_2Mn{\cdot}4H_2O$, Sigma-Aldrich) and citric acid (Sigma-Aldrich) in the molar ratio 1:1:1 was mixed in a rotary evaporator at 60°C until a gel was formed (after about 12 h of stirring). The gel was dried overnight in oven at 70°C, heated under air to 350°C with a rate of 2°C min^{-1}, and held 1 h at 350°C. The powder so obtained was ground in a mortar, heated under air to 550°C with a rate of 5°C min^{-1}, and held 10 h at 550°C to obtain the $LiMnPO_4$ phase. This sample (light gray powder in Fig. 1, following indicated by the acronym LMP) was afterwards carbon coated by pyrolysis procedure described in previous works [11,40]. The LMP powder was suspended in a sucrose (Sigma-Aldrich)/water solution (weight ratio LMP:sucrose = 80:20 %); the suspension was dried in a rotary evaporator at 60°C in order to precipitate a homogeneous sucrose layer over the olivine particles. The powder above obtained was heated under Ar flow to 700°C with a rate of 5°C min^{-1}, and held 3 h at 700°C to produce a carbon-$LiMnPO_4$ composite (black powder in Fig. 1, following indicated by the acronym LMP@C).

Thermogravimetric analysis (TGA; SDTA 851 Mettler-Toledo) was performed on LMP@C in a 60 ml min^{-1} air flow at a heating rate of 10°C min^{-1} from 25°C in order to estimate the carbon content. XRD experiments were carried out by using a Rigaku Xray Ultima$^+$ diffractometer equipped with a Cu Kα source and a graphite monocromator for the diffracted beam. The XRD

patterns refinement was performed by using the MAUD analysis software [41]. Samples morphology was investigated by scanning and transmission electron microscopies (SEM and TEM, respectively). SEM images were taken by a Zeiss EVO 40 microscope, equipped with a LaB_6 thermo-ionic electron gun. TEM images were taken by Zeiss EM 910 microscope, equipped with a tungsten thermo-ionic electron gun operating at 100 kV.

The cathode slurries were prepared by mixing active material, PVdF-HFP (Kynar Flex 2801) binder, and Super P Carbon (Timcal) conductive additive in tetrahydrofuran (THF, Sigma-Aldrich) in the weight ratio 80:10:10 %. The slurries were deposited on aluminum or carbon cloth current collectors by doctor blade and cast to obtain the electrode films. The cathode mass loading after vacuum drying overnight at 110°C was of about 4 mg cm^{-2}. Swagelok T-type lithium half-cells were assembled in Ar-filled glovebox by stacking the cathode, a Whatman glass math separator soaked in a 1 M $LiPF_6$ ethylene carbonate-dimethyl carbonate (EC-DMC) 1:1 by weight electrolyte solution (LP30, BASF), and a lithium foil counter electrode.

Galvanostatic cycling measurements were performed by using a Maccor Series 4000 battery test system. Li/LMP@C cells were cycled at room temperature (25°C) in the voltage range 2.5 − 4.6 V by following a constant current-constant voltage (CC-CV) procedure during charge, and a constant current (CC) procedure during discharge: charge and discharge were carried out at a CC of C/20 (1C = 170 mA g^{-1}), with a CV step at the end of charge at 4.6 V until a current value of C/50 was reached. Further galvanostatic cycling tests on Li/LMP@C cells were carried out at 70°C in the 2.5 – 4.5 V voltage range by using CC procedure at several current rates, i.e., C/5, C/3, C/2, and 1C (1C = 170 mA g^{-1}).

Electrochemical impedance spectroscopy (EIS) tests were carried out on a lithium half-cell at several states of charge obtained during a single CC-CV cycle. EIS spectra were recorded at OCV, at 4.3 V, at 4.6 V at the end of CC charge, at 4.6 V at the end of CV charge, at 3.96 V and 3.3 V during discharge, and at 2.5 V at the end of discharge. The EIS experiments during charge-discharge were performed through a VSP Bio-Logic multichannel potentiostat/galvanostat by

applying a 10 mV amplitude alternate signal in the frequency range 500 kHz – 20 mHz. The EIS spectra were analyzed by nonlinear least-square (NLLS) fit [42] using the Boukamp program.

Figure 1

Results and discussion

Structural disorder in the olivine lattice may partially hinder the lithium exchange ability within the [010] channels [15]. Meanwhile, post-synthesis annealing, widely used to improve the electrochemical performances, may induce slight structural changes within the olivine polyanionic network due to decrease of cationic disorder between lithium and transition metal [43,44]. Hence, XRD analysis has been performed before and after carbon coating in order to check the structural characteristics of the synthesized material. Fig. 2a shows the XRD patterns of LMP (red, bottom panel) and LMP@C (blue, top panel). Both patterns can be indexed to a single phase with olivine structure (space group Pmnb). Lattice parameters were calculated by Rietveld refinement of the experimental patterns (Fig. 2a; the continuous line represents the simulated pattern while the dots indicate the experimental pattern) basing on lithiophilite lattice ($LiMnPO_4$, 25834-ICSD) and reported in Table 1. The Rietveld analysis reveals only negligible change of the lattice upon sucrose pyrolysis at 700°C (see experimental section). After the annealing step, the LMP@C sample consist of a composite $LiMnPO_4$-C material containing about 3 wt.% of carbon, as confirmed by TGA (Fig. 2b).

Figure 2

Panels a-b, d-e of Fig. 3 report the SEM images of LMP (a, b) and LMP@C (d, e) at increasing magnifications. The images reveal for both samples aggregates of submicrometrical grains and limited differences in particle morphology, likely induced by the post-synthesis annealing. The micrometrical morphology may actually limit the electrolyte decomposition at the higher voltage values and advantageously increase the material tap density [45]. However, particles of excessively increased size generally hinder lithium diffusion within the material, thus limiting its electrochemical behavior. Indeed, suitable particle morphology is of key importance in order to

allow proper material operation in lithium cell [25]. TEM images of Fig. 3 (panels c, f) reveal that the aggregates shown by SEM are homogeneously formed by grains with average diameter below 100 nm. In addition, comparison of TEM of LMP (panel c) and LMP@C (panel f) indicates negligible particle size change upon annealing.

Figure 3

Following we omitted the electrochemical characterization of the bare olivine (LMP), that is not suitable electrode for our study, and focused the discussion on the carbon coated $LiMnPO_4$ sample (LMP@C) [12,22,24,46]. The electrochemical properties of the Li/LMP@C half-cell were studied by coupling a CC-CV cycling (see the experimental section for details) and EIS tests. A lithium half-cell was charged at CC from OCV (about 3 V) up to 4.6 V, held at CV of 4.6 V, and discharged down to 2.5 V. EIS analysis at several states of charge allowed investigation of the impedance features of the cell as well as determination of the lithium diffusion coefficient within the $LiMnPO_4$ electrode. Fig. 4 reports the voltage profile (a) and the related Nyquist plots obtained by EIS (b). The voltage values corresponding to each EIS experiment are pointed out by arrows in Fig. 4a. The figure shows a profile reflecting the Mn^{3+}/Mn^{2+} electrochemical process centered at about 4.1 V, with relatively high polarization between oxidation and reduction processes. The Nyquist plots (Fig. 4b) have been analyzed by nonlinear least-square (NLLS) fit [42] by using three different equivalent circuits, reported in inset of Fig. 4b. At OCV the cell shows a small semicircle at high frequency due to a passivation films formed at the electrodes, followed by a straight line related to the geometrical capacity of the cell, according to the equivalent circuit (1). At voltage values allowing the Mn^{3+}/Mn^{2+} electrochemical processes, i.e., 4 V to 4.6 V, the Nyquist plot shows a wider depressed semicircle at medium-high frequencies, followed by a tilted line having slope of approximately 45°. These impedance spectra have been fitted using the equivalent circuit (2): the depressed semicircle represents the convolution of passivation layers and charge transfer elements, while the tilted line is attributed to a Warburg element due to semi-infinite Li^+ diffusion within the LMP@C electrode. Decreasing voltage during discharge, i.e., 3.3 V to 2.5 V, leads to changes in

the slope of low-frequency line due to finite length effects on the diffusion [47]. This behavior is consistent with the impedance response of circuit (3). Fig. 4c shows the evolution of the interfacial resistance upon charge and discharge calculated by NLLS analysis of the EIS spectra. The figure indicates at OCV a passivation layer resistance of about 50 Ω. After charge at 4.3 V and current flow through the cell, the interfacial resistance increases to about 300 Ω owing to contribution of charge transfer at the electrodes/electrolyte interfaces and possible further growth of passivation layers. Afterwards, the above resistance decreases to about 200 Ω at 4.6 V and slightly increases upon CV step. During discharge, EIS reveals an interfacial resistance of about 250 Ω at 3.96 V, in correspondence to the Mn^{3+}/Mn^{2+} plateau, which increases to about 500 Ω at 3.3 V and then decreases to 400 Ω at 2.5 V. Several contributions may account for the interfacial resistance change during cell operation, among them: (i) passivation layer growth leading to resistance increase, (ii) variation of charge transfer resistance due to voltage and state-of-charge changes, (iii) possible passivation layer dissolution leading to resistance decrease.

Fig. 4d shows the cell voltage vs. specific capacity of three cycles obtained by CC-CV procedure (see discussion of Fig. 4a and experimental section). The profile shows a main plateau centered at 4.1 V attributed to Mn^{3+}/Mn^{2+} redox process and charge-discharge polarization of about 0.2 V. The electrode delivers a specific discharge capacity of 104 mAh g^{-1}, i.e., about 61 % of the theoretical value for the material, with a coulombic efficiency of 87 %. Despite a slight decrease of the delivered capacity, the charge discharge efficiency increases to about 92 % by the following cycles. As introduced in this work, the relatively low capacity and efficiency values observed for the material may be attributed to hindered reversible Li^+ (de)insertion though the electrode mainly due to insulator features leading to low ion diffusion ability [20,28,29]. Therefore, following we report a study suitable for better understanding the lithium diffusion characteristics within the LMP@C material.

Figure 4

The lithium diffusion properties of the LMP@C electrodes were evaluated by analyzing the EIS data of Fig. 4b using the following equation [40,48,49]:

$$D_{Li^+} = \frac{1}{2}\left(\frac{RT}{z^2F^2CA\sigma}\right)^2 \quad (1)$$

where R is the gas constant (8.314 J K^{-1} mol^{-1}), T is the temperature (298 K), z = 1 is the number of exchanged electrons, F is the Faraday constant (96485 C mol^{-1}), C is the Li^+ concentration within the $LiMnPO_4$ lattice (mol cm^{-3}), which varies during (de)lithiation, and A is the electrode geometric area (0.785 cm^2). σ is the pre-exponential factor in the equation of the complex impedance vs. frequency (ω) within the semi-infinite diffusion condition (Z_W^*) [47]:

$$Z_W^* = \sigma\omega^{-1/2} - j\sigma\omega^{-1/2} \quad (2)$$

Accordingly, σ was determined by linear interpolation of the plots reported in Fig. 5, in which the real and imaginary components of Z^* in the Warburg region (i.e., Z' and Z'', respectively) were reported as function of $\omega^{-1/2}$. The figure reveals both for Z' and for Z'' a linear trend vs. $\omega^{-1/2}$ with the same slope (σ) within the experimental error, thus confirming the mentioned semi-infinite diffusion condition. Hence, we calculated D_{Li^+} by applying equation (1) using the above obtained σ, related to the impedance spectra of Fig. 4b, i.e., by cell operation. This approach allowed the evaluation of the lithium diffusion coefficient by changing the material state of charge. Previous works [30,31,33,35–40] reported diffusion coefficient as determined by EIS for $LiMnPO_4$ materials synthesized by several approaches. However, most of them studied D_{Li^+} by EIS of fully lithiated $LiMnPO_4$ electrodes. Wang et al. [30] and Zhang et al. [39] reported lithium diffusion coefficients of 5×10^{-14} cm^2 s^{-1} and 8×10^{-14} cm^2 s^{-1}, respectively, for solvothermally prepared $LiMnPO_4$ materials. Fang et. al [31] measured D_{Li^+} of 2×10^{-14} cm^2 s^{-1} in $LiMnPO_4$ obtained by solid-state approach. Ramar et al. [36] investigated the effect of the high-energy ball milling time on the lithium diffusion properties in $LiMnPO_4$ synthesized by a soft template method. They showed that milling time affect the electrochemically evaluated lithium diffusion coefficient, reporting D_{Li^+} within the $10^{-16} - 10^{-13}$ cm^2 s^{-1} range. Furthermore, slight variation of D_{Li^+} within the 2×10^{-14} –

6×10^{-14} cm^2 s^{-1} range was measured in different $LiMnPO_4$ samples prepared by co-precipitation synthesis using several calcination temperatures from 550°C to 700°C [38]. Further literature works reported lithium diffusion coefficient by EIS of partially lithiated $LiMnPO_4$. We evaluated in a recent paper that D_{Li^+} during charge and following discharge of solvothermally synthesized $LiMnPO_4$ may range within $10^{-13} - 10^{-12}$ cm^2 s^{-1} [40]. Furthermore, Zhou et al. measured D_{Li^+} at half-charge within the $10^{-16} - 10^{-14}$ cm^2 s^{-1} range for several $LiMnPO_4$ materials prepared by using different manganese precursors in the solvothermal recipe [37].

Figure 5

Fig. 6a shows D_{Li^+} (top panel) at several states of charge and related position on the voltage profile during charge-discharge (bottom panel) of the material studied in this work. The figure reveals lithium diffusion coefficient slightly varying within the $10^{-14} - 10^{-13}$ cm^2 s^{-1} range. In particular, D_{Li^+} shows a decreasing trend during charge from 8×10^{-14} cm^2 s^{-1} at 4.3 V (corresponding to the Mn^{2+}/Mn^{3+} plateau), to 7×10^{-14} cm^2 s^{-1} at 4.6 V (end of CC charge), and to 6×10^{-14} cm^2 s^{-1} at 4.6 V (end of the CV step). During discharge, D_{Li^+} further decreases to 5×10^{-14} cm^2 s^{-1} at 3.96 V (Mn^{2+}/Mn^{3+} plateau), 2×10^{-14} cm^2 s^{-1} at 3.3 V, and finally stabilizes at 2×10^{-14} cm^2 s^{-1} at 2.5 V (end of discharge). A previous paper revealed the strong dependence of D_{Li^+}, as measured by EIS, on the state of charge using a hydrothermally prepared $LiMnPO_4$ material [35]. The study evidenced D_{Li^+} values of 4×10^{-16} cm^2 s^{-1} and 5×10^{-17} cm^2 s^{-1} for fully discharged and fully charged electrodes, respectively, while significantly lower D_{Li^+} values, i.e., 9×10^{-21} cm^2 s^{-1} and 3×10^{-18} cm^2 s^{-1}, were reported for 60 % and 30 % states of charge, respectively. Furthermore, a $LiMnPO_4$ material prepared by solid-state approach has shown a lithium diffusion coefficient ranging from 10^{-11} to 10^{-13} cm^2 s^{-1} at various state of charges [33].

These data indicate that relevant changes of the lithium transport properties in $LiMnPO_4$ samples are attributed to the synthesis procedure, which strongly affects the structural and morphological features of the cathode. Despite the limited variation of the lithium transport properties of the material observed throughout operation in lithium cell, it is noteworthy that our

study reveals lithium diffusion coefficient values consistent with those already reported in previous investigations. However, significant change of the lithium diffusion coefficient cannot be excluded for x > 0.7 in $xMnPO_4/(1-x)LiMnPO_4$, which is the maximum delithiation degree estimated by galvanostatic cycling (Fig. 4d) and represented in the scheme of Fig. 6a (bottom panel, end of charge). Further effect on D_{Li^+} may be attributed to incomplete discharge process (scheme of Fig. 6a, end of discharge), and requires further investigation to be fully clarified.

Figure 6

The results herein reported agrees with current literature works suggesting the hindered kinetics of lithium insertion/deinsertion for $LiMnPO_4$ materials with respect to $LiFePO_4$ [19–21]. This severe issue represents the main problem limiting the effective employment of Mn-based olivines as cathodes in lithium battery. The increase of operating temperature may actually favor the Li^+ transport ability of olivine materials, thus improving the electrochemical performances, even at the higher currents [50–52]. This trend is confirmed by the cycling tests performed at 70°C shown by Fig. 6a, which clearly reveal the beneficial effect of the temperature increase on $LiMnPO_4$ electrochemical properties. Indeed, the voltage profiles at increasing several current rates of Fig. 6b show remarkable enhancement with respect to the electrochemical performance at room temperature (compare with Fig. 4d). The electrode delivers reversible capacity of 127, 112, 98, and 90 mAh g^{-1} at C/5, C/3, C/2, and 1C rates (1C = 170 mA g^{-1}), respectively (see Fig. 6b), however with lower coulombic efficiency during the first cycles, i.e., within the 85 – 88 % range, attributed to side electrolyte decomposition favored by the higher temperature. Nevertheless, Fig. 6c indicates reversible operation of $LiMnPO_4$ at C/2 rate after the 1st cycle, with voltage profiles centered at 4.1 V, discharge capacity of about 104 mAh g^{-1}, and charge-discharge polarization of about 0.18 V. The cell shows a relatively stable cycling trend and coulombic efficiency approaching 96 % after 30 cycles, as confirmed by Fig. 6d.

Conclusion

We characterized a $LiMnPO_4$ electrode prepared by sol-gel technique and coated by 3 wt.% of carbon. The olivine material was formed by aggregates of submicrometrical grains (< 100 nm), which underwent minor structural and morphological changes upon carbon coating. The study in lithium cell revealed reversible lithium (de-)insertion into the olivine, a de-lithiation degree of about 70 %, and EIS response including passivation layers, charge transfer process, semi-infinite lithium diffusion into $LiMnPO_4$, as well as finite length effects. The results indicated lithium diffusion coefficient slightly varying within the $10^{-14} - 10^{-13}$ cm^2 s^{-1} range at several states of charge. Comparison of these values with literature reports suggested that the lithium diffusion coefficient evaluation is strongly affected by *(i)* the structural and morphological characteristics of the material due to the synthesis procedure, *(ii)* the adopted experimental setup used for evaluation. The electrode kinetics in lithium cells are significantly enhanced by rising temperature to 70°C, thus leading to reversible operation at a c-rate as high C/2 (1C = 170 mA g^{-1}) with discharge capacity approaching 100 mAh g^{-1}.

Acknowledgements

The work was performed within the collaboration project "Accordo di Collaborazione Quadro 2015" between University of Ferrara (Department of Chemical and Pharmaceutical Sciences) and Sapienza University of Rome (Chemistry Department). The authors thank Daniela Palmeri (Electronic Microscopy Centre, Department of Chemical and Pharmaceutical Sciences) University of Ferrara, Italy) for performing SEM and TEM images.

References

[1] A.K. Padhi, K.S. Nanjundaswamy, J.B. Goodenough, Phospho-olivines as Positive-Electrode Materials for Rechargeable Lithium Batteries, J. Electrochem. Soc. 144 (1997) 1188–1194.

[2] A.K. Padhi, Effect of Structure on the Fe^{3+}/Fe^{2+} Redox Couple in Iron Phosphates, J. Electrochem. Soc. 144 (1997) 1609. doi:10.1149/1.1837649.

[3] A. Yamada, S.C. Chung, K. Hinokuma, Optimized $LiFePO_4$ for Lithium Battery Cathodes, J. Electrochem. Soc. 148 (2001) A224. doi:10.1149/1.1348257.

[4] Z. Chen, J.R. Dahn, Reducing Carbon in $LiFePO_4$/C Composite Electrodes to Maximize Specific Energy, Volumetric Energy, and Tap Density, J. Electrochem. Soc. 149 (2002) A1184. doi:10.1149/1.1498255.

[5] S.-Y. Chung, J.T. Bloking, Y.-M. Chiang, Electronically conductive phospho-olivines as lithium storage electrodes., Nat. Mater. 1 (2002) 123–128. doi:10.1038/nmat732.

[6] F. Croce, A. D' Epifanio, J. Hassoun, A. Deptula, T. Olczac, B. Scrosati, A Novel Concept for the Synthesis of an Improved $LiFePO_4$ Lithium Battery Cathode, Electrochem. Solid-State Lett. 5 (2002) A47. doi:10.1149/1.1449302.

[7] J. Jiang, J.R. Dahn, ARC studies of the thermal stability of three different cathode materials: $LiCoO_2$; $Li[Ni_{0.1}Co_{0.8}Mn_{0.1}]O_2$; and $LiFePO_4$, in $LiPF_6$ and LiBOB EC/DEC electrolytes, Electrochem. Commun. 6 (2004) 39–43. doi:10.1016/j.elecom.2003.10.011.

[8] Y. Wang, P. He, H. Zhou, Olivine $LiFePO_4$: development and future, Energy Environ. Sci. 4 (2011) 805. doi:10.1039/c0ee00176g.

[9] K. Zaghib, A. Guerfi, P. Hovington, A. Vijh, M. Trudeau, A. Mauger, J.B. Goodenough, C.M. Julien, Review and analysis of nanostructured olivine-based lithium recheargeable batteries: Status and trends, J. Power Sources. 232 (2013) 357–369. doi:10.1016/j.jpowsour.2012.12.095.

[10] K. Amine, H. Yasuda, M. Yamachi, Olivine $LiCoPO_4$ as 4.8 V Electrode Material for Lithium Batteries, Electrochem. Solid-State Lett. 3 (2000) 178–179. doi:10.1149/1.1390994.

[11] D. Di Lecce, R. Brescia, A. Scarpellini, M. Prato, J. Hassoun, A High Voltage Olivine Cathode for Application in Lithium-Ion Batteries, ChemSusChem. 9 (2016) 223–230. doi:10.1002/cssc.201501330.

[12] G. Li, H. Azuma, M. Tohda, $LiMnPO_4$ as the Cathode for Lithium Batteries, Electrochem. Solid-State Lett. 5 (2002) A135. doi:10.1149/1.1475195.

[13] J. Wolfenstine, J. Allen, Ni^{3+}/Ni^{2+} redox potential in $LiNiPO_4$, J. Power Sources. 142 (2005) 389–390. doi:10.1016/j.jpowsour.2004.11.024.

[14] S. Brutti, J. Manzi, A. De Bonis, D. Di Lecce, F. Vitucci, A. Paolone, F. Trequattrini, S. Panero, Controlled synthesis of $LiCoPO_4$ by a solvo-thermal method at 220°C, Mater. Lett. 145 (2015) 324–327. doi:10.1016/j.matlet.2015.01.137.

[15] D. Di Lecce, J. Manzi, F.M. Vitucci, A. De Bonis, S. Panero, S. Brutti, Effect of the iron doping in $LiCoPO_4$ cathode materials for lithium cells, Electrochim. Acta. 185 (2015) 17–27. doi:10.1016/j.electacta.2015.10.107.

[16] D. Di Lecce, S. Brutti, S. Panero, J. Hassoun, A new Sn-C/$LiFe_{0.1}Co_{0.9}PO_4$ full lithium-ion cell with ionic liquid-based electrolyte, Mater. Lett. 139 (2015) 329–332. doi:10.1016/j.matlet.2014.10.089.

[17] V. Aravindan, J. Gnanaraj, Y.-S. Lee, S. Madhavi, $LiMnPO_4$ – A next generation cathode material for lithium-ion batteries, J. Mater. Chem. A. 1 (2013) 3518–3539. doi:10.1039/c2ta01393b.

[18] D. Di Lecce, C. Fasciani, B. Scrosati, J. Hassoun, A Gel–Polymer Sn–C/$LiMn_{0.5}Fe_{0.5}PO_4$ Battery Using a Fluorine-Free Salt, ACS Appl. Mater. Interfaces. 7 (2015) 21198–21207. doi:10.1021/acsami.5b05179.

[19] A. Yamada, M. Hosoya, S.C. Chung, Y. Kudo, K. Hinokuma, K.Y. Liu, Y. Nishi., Olivine-type cathodes: Achievements and problems, J. Power Sources. 119–121 (2003) 232–238. doi:10.1016/S0378-7753(03)00239-8.

[20] M. Yonemura, A. Yamada, Y. Takei, N. Sonoyama, R. Kanno, Comparative Kinetic Study of Olivine Li_xMPO_4 (M=Fe, Mn), J. Electrochem. Soc. 151 (2004) A1352. doi:10.1149/1.1773731.

[21] A. Yamada, Y. Takei, H. Koizumi, N. Sonoyama, R. Kanno, K. Itoh, M. Yonemura, T. Kamiyama, Electrochemical, Magnetic, and Structural Investigation of the $Li_x(Mn_yFe_{1-y})PO_4$ Olivine Phases, Chem. Mater. 18 (2006) 804–813. doi:10.1021/cm051861f.

[22] S.M. Oh, S.W. Oh, C.S. Yoon, B. Scrosati, K. Amine, Y.K. Sun, High-performance carbon-$LiMnPO_4$ nanocomposite cathode for lithium batteries, Adv. Funct. Mater. 20 (2010) 3260–3265. doi:10.1002/adfm.201000469.

[23] D. Choi, D. Wang, I.T. Bae, J. Xiao, Z. Nie, W. Wang, V.V. Viswanathan, Y.J. Lee, J.-G. Zhang, G.L. Graff, Z. Yang, J. Liu, $LiMnPO_4$ nanoplate grown via solid-state reaction in molten hydrocarbon for Li-ion battery cathode, Nano Lett. 10 (2010) 2799–2805. doi:10.1021/nl1007085.

[24] Z. Bakenov, I. Taniguchi, Electrochemical performance of nanocomposite $LiMnPO_4$/C cathode materials for lithium batteries, Electrochem. Commun. 12 (2010) 75–78. doi:10.1016/j.elecom.2009.10.039.

[25] T. Drezen, N.H. Kwon, P. Bowen, I. Teerlinck, M. Isono, I. Exnar, Effect of particle size on $LiMnPO_4$ cathodes, J. Power Sources. 174 (2007) 949–953. doi:10.1016/j.jpowsour.2007.06.203.

[26] S.M. Oh, S.W. Oh, S.T. Myung, S.M. Lee, Y.K. Sun, The effects of calcination temperature on the electrochemical performance of $LiMnPO_4$ prepared by ultrasonic spray pyrolysis, J. Alloys Compd. 506 (2010) 372–376. doi:10.1016/j.jallcom.2010.07.010.

[27] M. Michalska, L. Lipińska, A. Sikora, D. Ziółkowska, K.P. Korona, M. Andrzejczuk, Structural and morphological studies of manganese-based cathode materials for lithium ion batteries, J. Alloys Compd. 632 (2015) 256–262. doi:10.1016/j.jallcom.2014.12.266.

[28] D. Wang, C. Ouyang, T. Drézen, I. Exnar, A. Kay, N.-H. Kwon, P. Gouerec, J. H. Miners, M. Wang, M. Grätzel, Improving the Electrochemical Activity of $LiMnPO_4$ Via Mn-Site Substitution, J. Electrochem. Soc. 157 (2010) A225. doi:10.1149/1.3271112.

[29] S.P. Ong, V.L. Chevrier, G. Ceder, Comparison of small polaron migration and phase separation in olivine $LiMnPO_4$ and $LiFePO_4$ using hybrid density functional theory, Phys. Rev. B - Condens. Matter Mater. Phys. 83 (2011) 1–7. doi:10.1103/PhysRevB.83.075112.

[30] Y. Wang, Y. Yang, Y. Yang, H. Shao, Enhanced electrochemical performance of unique

morphological cathode material prepared by solvothermal method, Solid State Commun. 150 (2010) 81–85. doi:10.1016/j.ssc.2009.09.046.

[31] H. Fang, H. Yi, C. Hu, B. Yang, Y. Yao, W. Ma, Y. Dai., Effect of Zn doping on the performance of $LiMnPO_4$ cathode for lithium ion batteries, Electrochim. Acta. 71 (2012) 266–269. doi:10.1016/j.electacta.2012.03.160.

[32] H. Manjunatha, T. V. Venkatesha, G.S. Suresh, Electrochemical studies of $LiMnPO_4$ as aqueous rechargeable lithium–ion battery electrode, J. Solid State Electrochem. 16 (2012) 1941–1952. doi:10.1007/s10008-011-1593-3.

[33] H. Manjunatha, K.C. Mahesh, G.S. Suresh, T.V. Venkatesha, Kinetics of lithium insertion into $LiMnPO_4$ from aqueous saturated LiOH: A study using galvanostatic and potentiostatic intermittent titration techniques, Electrochim. Acta. 80 (2012) 269–281. doi:10.1016/j.electacta.2012.07.003.

[34] Y. Cao, J. Duan, G. Hu, F. Jiang, Z. Peng, K. Du, H. Guo, Synthesis and electrochemical performance of nanostructured $LiMnPO_4$/C composites as lithium-ion battery cathode by a precipitation technique, Electrochim. Acta. 98 (2013) 183–189. doi:10.1016/j.electacta.2013.03.014.

[35] H.-C. Dinh, S. Mho, Y. Kang, I.-H. Yeo, Large discharge capacities at high current rates for carbon-coated $LiMnPO_4$ nanocrystalline cathodes, J. Power Sources. 244 (2013) 189–195. doi:10.1016/j.jpowsour.2013.01.191.

[36] V. Ramar, K. Saravanan, S.R. Gajjela, S. Hariharan, P. Balaya, The effect of synthesis parameters on the lithium storage performance of $LiMnPO_4$/C, Electrochim. Acta. 105 (2013) 496–505. doi:10.1016/j.electacta.2013.05.025.

[37] F. Zhou, P. Zhu, X. Fu, R. Chen, R. Sun, C. Wong, Comparative study of $LiMnPO_4$ cathode materials synthesized by solvothermal methods using different manganese salts, CrystEngComm. 16 (2014) 766–774. doi:10.1039/C3CE41567H.

[38] H.-J. Zhu, W. Zhai, M. Yang, X. Liu, Y.-C. Chen, H. Yang, X.-d. Shen, Synthesis and

characterization of $LiMnPO_4$/C nano-composites from manganese(ii) phosphate trihydrate precipitated from a micro-channel reactor approach, RSC Adv. 4 (2014) 25625. doi:10.1039/c4ra01943a.

[39] Z. Zhang, G. Hu, Y. Cao, J. Duan, K. Du, Z. Peng, Enhanced electrochemical performance of nano $LiMnPO_4$ with multifunctional surface co-coating of Li_2TiO_3 and carbon, Solid State Ionics. 283 (2015) 115–122. doi:10.1016/j.ssi.2015.10.007.

[40] D. Di Lecce, J. Hassoun, Lithium Transport Properties in $LiMn_{1-\alpha}Fe_{\alpha}PO_4$ Olivine Cathodes, J. Phys. Chem. C. 119 (2015) 20855–20863. doi:10.1021/acs.jpcc.5b06727.

[41] L. Lutterotti, Total pattern fitting for the combined size–strain–stress–texture determination in thin film diffraction, Nucl. Instruments Methods Phys. Res. Sect. B Beam Interact. with Mater. Atoms. 268 (2010) 334–340. doi:10.1016/j.nimb.2009.09.053.

[42] B.A. Boukamp, A Nonlinear Least Squares Fit procedure for analysis of immittance data of electrochemical systems, Solid State Ionics. 20 (1986) 31–44. doi:10.1016/0167-2738(86)90031-7.

[43] J. Chen, J. Graetz, Study of antisite defects in hydrothermally prepared $LiFePO_4$ by in situ x-ray diffraction, ACS Appl. Mater. Interfaces. 3 (2011) 1380–1384. doi:10.1021/am200141a.

[44] J. Chen, M.S. Whittingham, Hydrothermal synthesis of lithium iron phosphate, Electrochem. Commun. 8 (2006) 855–858. doi:10.1016/j.elecom.2006.03.021.

[45] S.-M. Oh, S.-T. Myung, J.B. Park, B. Scrosati, K. Amine, Y.-K. Sun, Double-structured $LiMn_{(0.85)}Fe_{(0.15)}PO_4$ coordinated with $LiFePO_4$ for rechargeable lithium batteries., Angew. Chemie Int. Ed. 51 (2012) 1853–6. doi:10.1002/ange.201107394.

[46] S.K. Martha, B. Markovsky, J. Grinblat, Y. Gofer, O. Haik, E. Zinigrad, et al., $LiMnPO_4$ as an Advanced Cathode Material for Rechargeable Lithium Batteries, J. Electrochem. Soc. 156 (2009) A541. doi:10.1149/1.3125765.

[47] C. Ho, Application of A-C Techniques to the Study of Lithium Diffusion in Tungsten Trioxide Thin Films, J. Electrochem. Soc. 127 (1980) 343. doi:10.1149/1.2129668.

[48] J. Hassoun, R. Verrelli, P. Reale, S. Panero, G. Mariotto, S. Greenbaum, et al., A structural, spectroscopic and electrochemical study of a lithium ion conducting $Li_{10}GeP_2S_{12}$ solid electrolyte, J. Power Sources. 229 (2013) 117–122. doi:10.1016/j.jpowsour.2012.11.130.

[49] F. Gao, Z. Tang, Kinetic behavior of $LiFePO_4$/C cathode material for lithium-ion batteries, Electrochim. Acta. 53 (2008) 5071–5075. doi:10.1016/j.electacta.2007.10.069.

[50] A.S. Andersson, Thermal Stability of $LiFePO_4$-Based Cathodes, Electrochem. Solid-State Lett. 3 (1999) 66. doi:10.1149/1.1390960.

[51] X.H. Rui, Y. Jin, X.Y. Feng, L.C. Zhang, C.H. Chen, A comparative study on the low-temperature performance of $LiFePO_4$/C and $Li_3V_2(PO_4)_3$/C cathodes for lithium-ion batteries, J. Power Sources. 196 (2011) 2109–2114. doi:10.1016/j.jpowsour.2010.10.063.

[52] F. Wang, J. Chen, Z. Tan, M. Wu, B. Yi, W. Su, et al., Low-temperature electrochemical performances of $LiFePO_4$ cathode materials for lithium ion batteries, J. Taiwan Inst. Chem. Eng. 45 (2014) 1321–1330. doi:10.1016/j.jtice.2014.02.013.

Table caption

Table 1. Lattice parameters obtained by Rietveld refinement of LMP and LMP@C.

Figure captions

Figure 1. Photographic images of bare $LiMePO_4$ sample (light gray powder) indicated by the acronym LMP and carbon coated $LiMePO_4$ sample (black powder) indicated by the acronym LMP@C in this work.

Figure 2. (**a**) X-ray diffraction (XRD) patterns of pristine (LMP, red) and C-coated (LMP@C, blue) samples. Experimental patterns reported as dots and calculated patterns basing on $LiMnPO_4$ lithiophilite lattice (25834-ICSD, space group Pmnb) reported as continuous line. (**b**) Thermogravimetric analysis (TGA) performed on LMP@C in a 60 ml min^{-1} air flow at a heating rate of 10°C min^{-1} from 25°C.

Figure 3. Scanning electron micrographs (SEMs) at increasing magnifications of (**a**, **b**) pristine (LMP) and (**d**, **e**) C-coated (LMP@C) samples. Transmission electron micrographs (TEMs) of (**c**) pristine (LMP) and (**f**) C-coated (LMP@C) samples.

Figure 4. (**a**) Voltage profiles of the C-coated $LiMnPO_4$ (LMP@C) electrode cycled in lithium half-cell by following a constant current-constant voltage (CC-CV) procedure during charge and a CC procedure during discharge (2.5 − 4.6 V voltage range; CC of C/20; current limit of C/50 for CV step; 1C = 170 mA g^{-1}). (**b**) Nyquist plots from EIS spectra of the LMP@C/Li cell recorded at several states of charge; 10 mV amplitude alternate signal in the frequency range 500 kHz – 20 mHz; **inset**: equivalent circuits used for NNLS analysis. (**c**) Evolution of the interfacial resistance and related components (R_1 and R_2, see equivalent circuits of panel **b**) calculated by NLLS analysis of the EIS spectra. (**d**) Cell voltage vs. specific capacity of the LMP@C/Li cell in three cycles obtained by using the CC-CV procedure (2.5 − 4.6 V voltage range; CC of C/20; current limit of C/50 for CV step; 1C = 170 mA g^{-1}).

Figure 5. Plots of the real and imaginary components of Z^* (Z' and Z'', respectively) vs. $\omega^{-1/2}$ in the Warburg region for the EIS spectra of Fig. 3 and related linear fit. Plots related to the EIS at (**a**) 4.3 V during charge, (**b**) 4.6 V at the end of charge, (**c**) 4.6 V at the end of CV, (**d**) 3.96 V and (**e**) 3.3 V during discharge, and (**f**) 2.5 V at the end of discharge.

Figure 6. (**a**) Evolution of the lithium diffusion coefficient (D_{Li^+}) by changing the state of charge from analysis of the EIS spectra of Fig. 3. **Top panel**: lithium diffusion coefficient; **bottom panel**: related position on the voltage profile and schematic representation of the $MnPO_4/LiMnPO_4$ ratio. (**b-d**) Galvanostatic cycling of C-coated $LiMnPO_4$ (LMP@C) electrode cycled in lithium half-cell at 70°C in the 2.5 – 4.5 V voltage range by using CC procedure; (**b**) voltage profiles at C/5, C/3, C/2, and 1C rates; (**c**) voltage profiles and (**d**) corresponding cycling behavior at C/2 rate (1C = 170 mA g^{-1}).

Graphical abstract

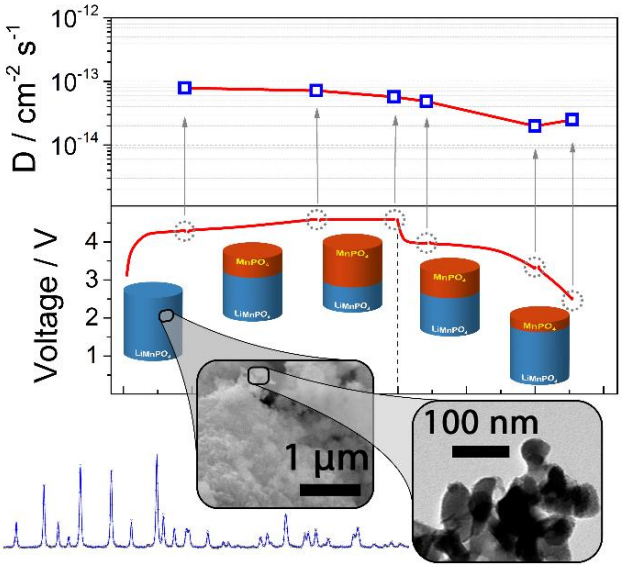

Highlights

- $LiMnPO_4$ electrode is prepared by a sol-gel synthesis
- The lithium diffusion characteristics of the material are studied
- Electrochemical impedance spectroscopy is performed at several states of charge
- The lithium diffusion coefficient varies within 10^{-14} and 10^{-13} cm^2 s^{-1}
- Tests at 70^{o}C reveal remarkable enhancement due to improved electrode kinetics

Table

Sample	a/Å	b/Å	c/Å	V/Å^3
LMP	6.1046 ±0.0005	10.450 ± 0.001	4.7443 ± 0.0005	302.64 ± 0.09
LMP@C	6.1039 ± 0.0004	10.4479 ± 0.0008	4.7432 ± 0.0004	302.49 ± 0.07

Table 1

Figure 1

Figure 1

Figure 2

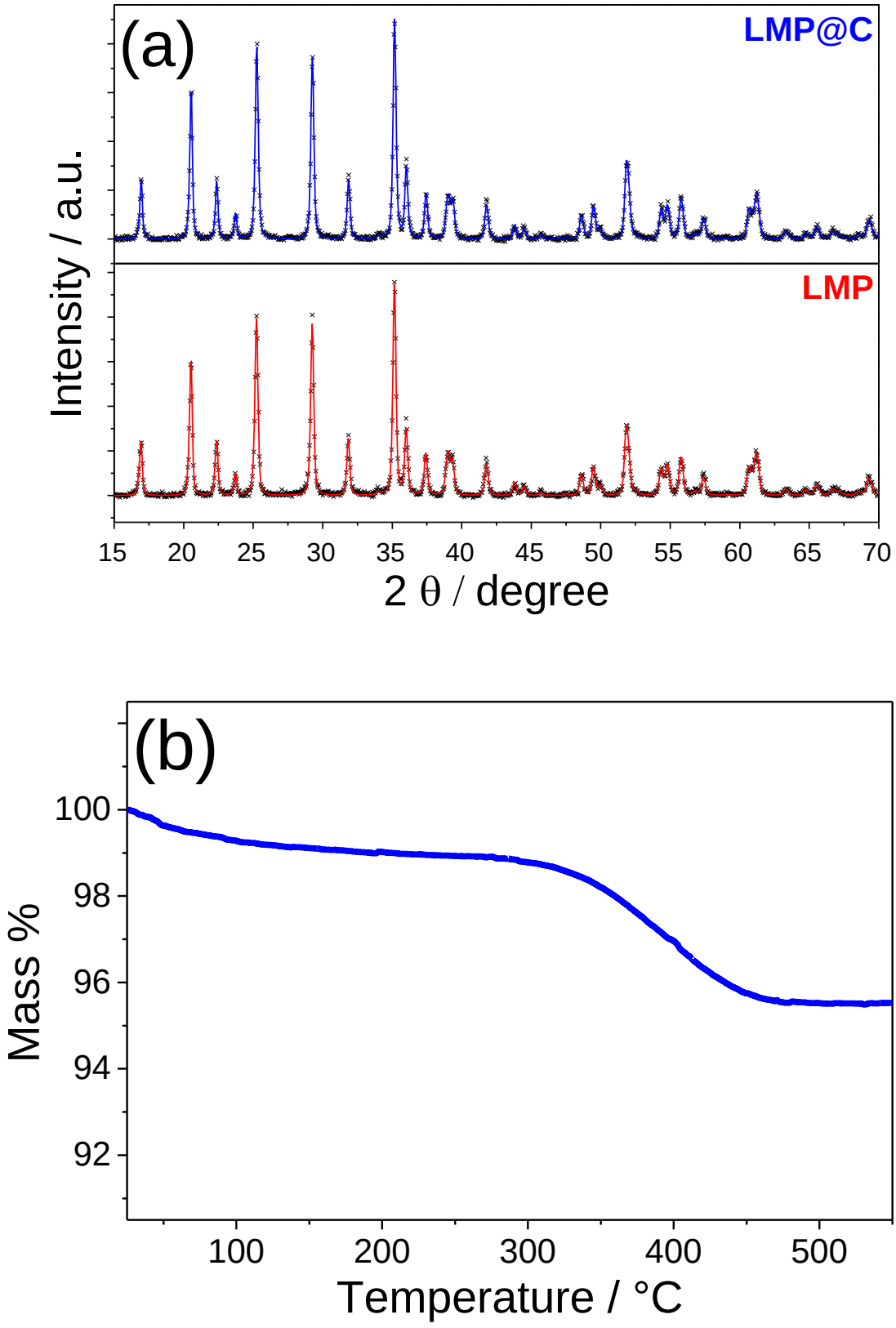

Figure 2

Figure 3

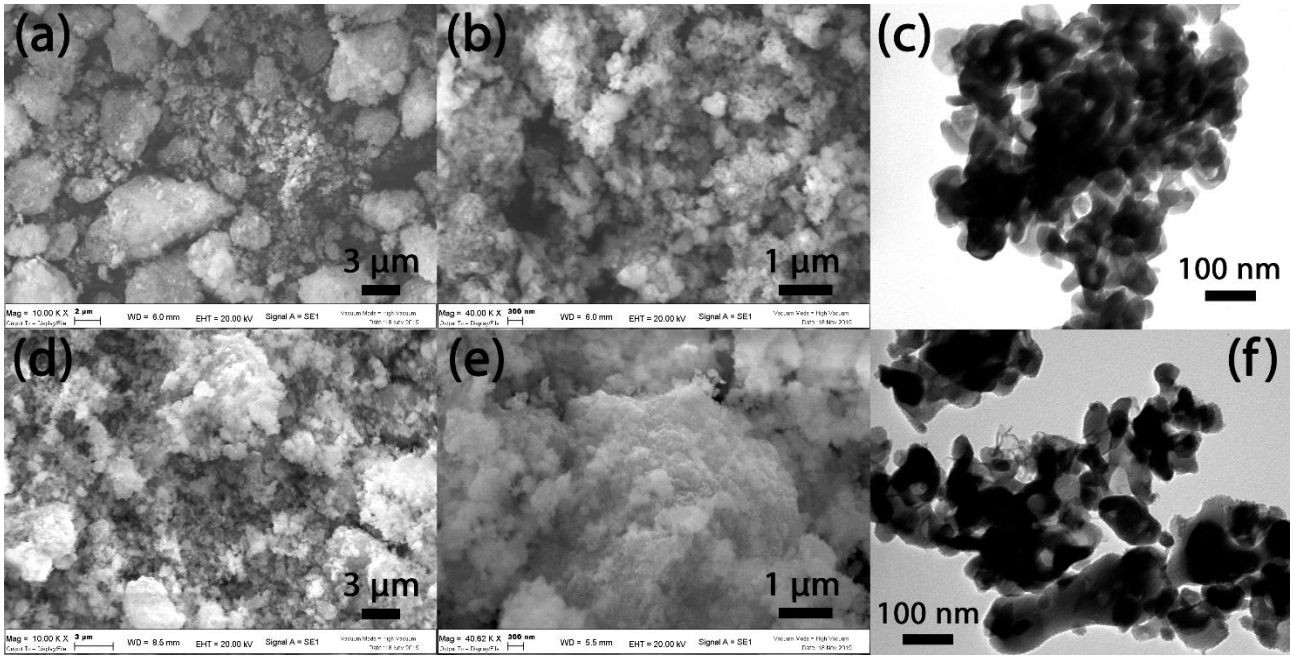

Figure 3

Figure 4 revised

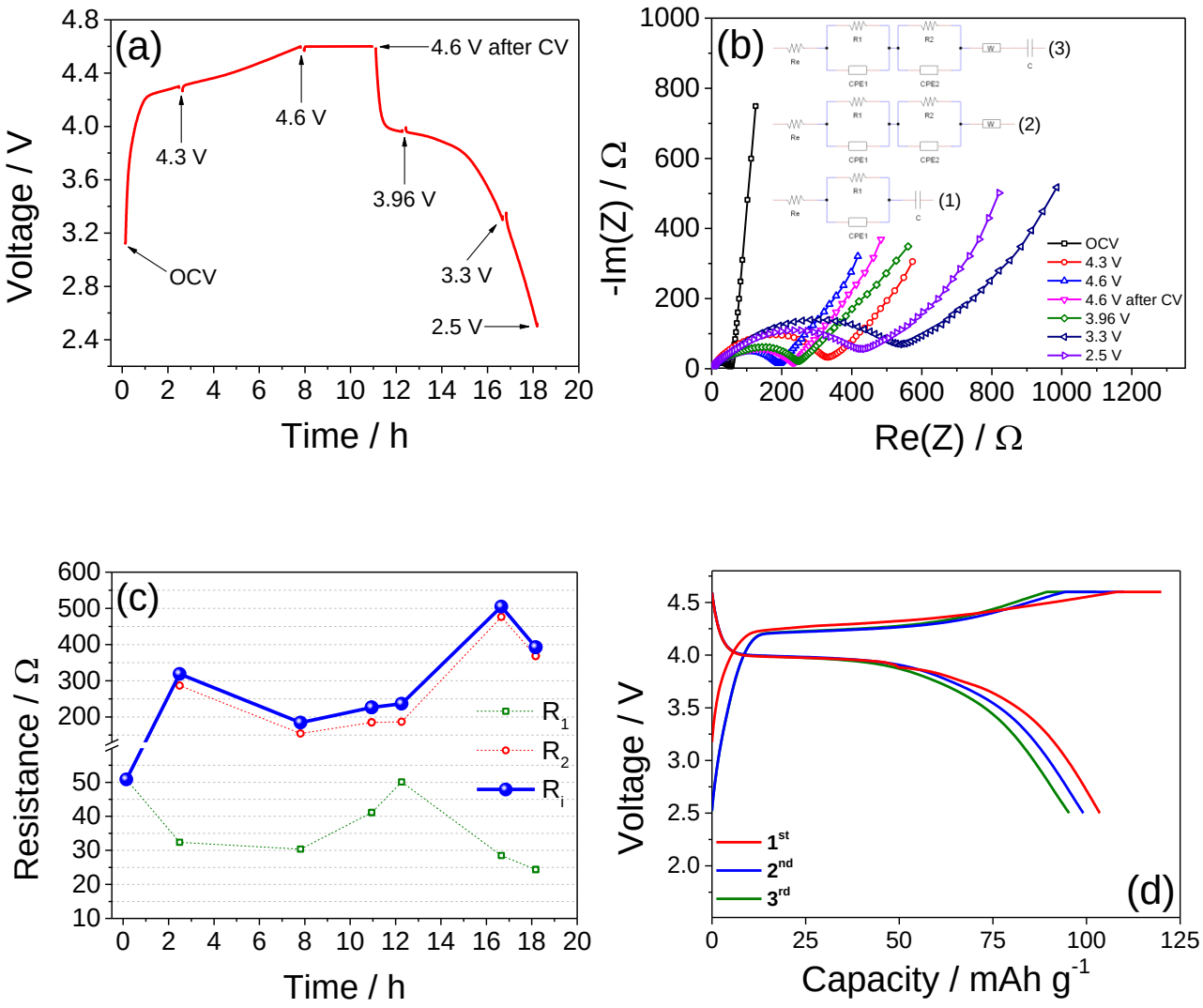

Figure 4

Figure 5

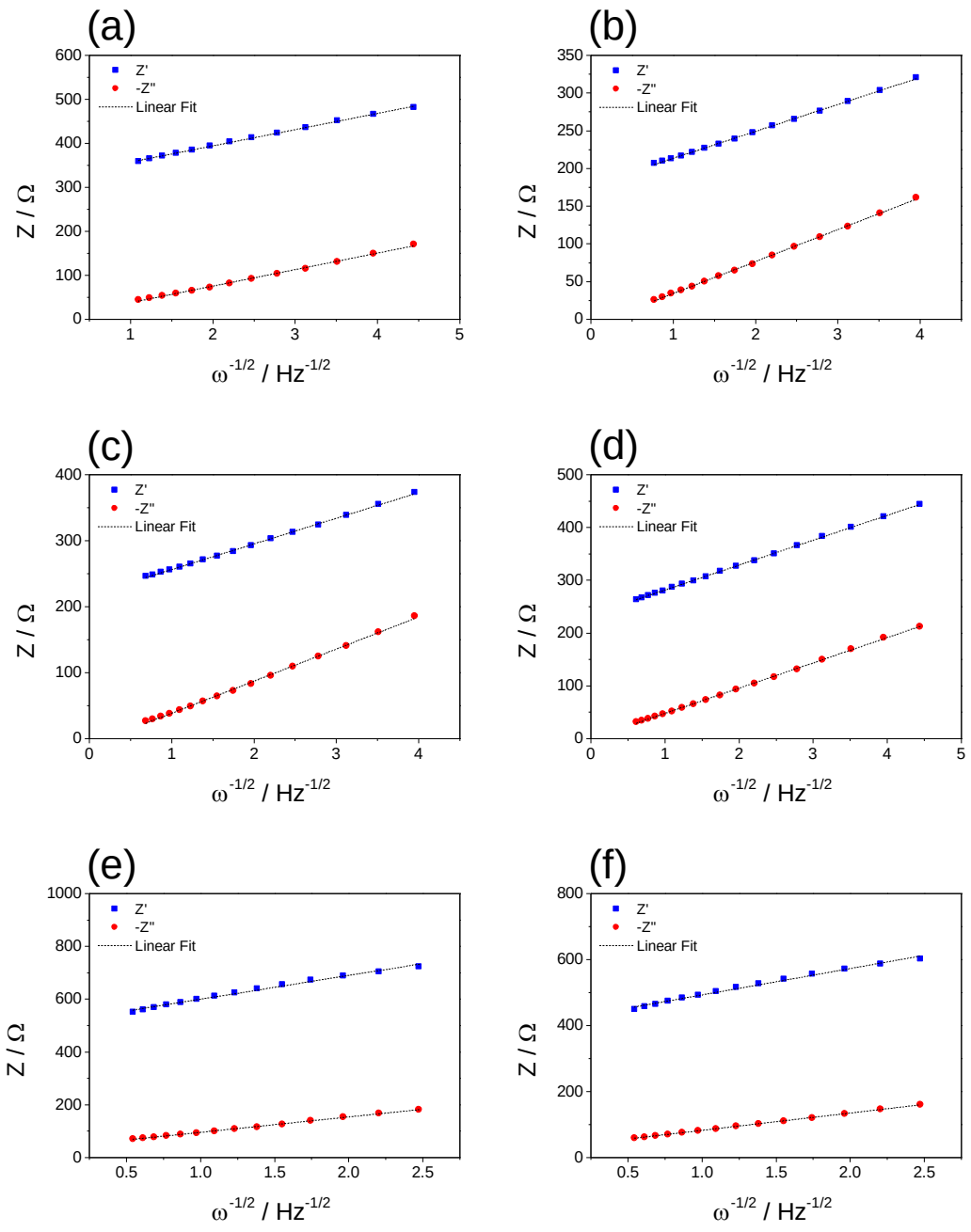

Figure 5

Figure 6 revised

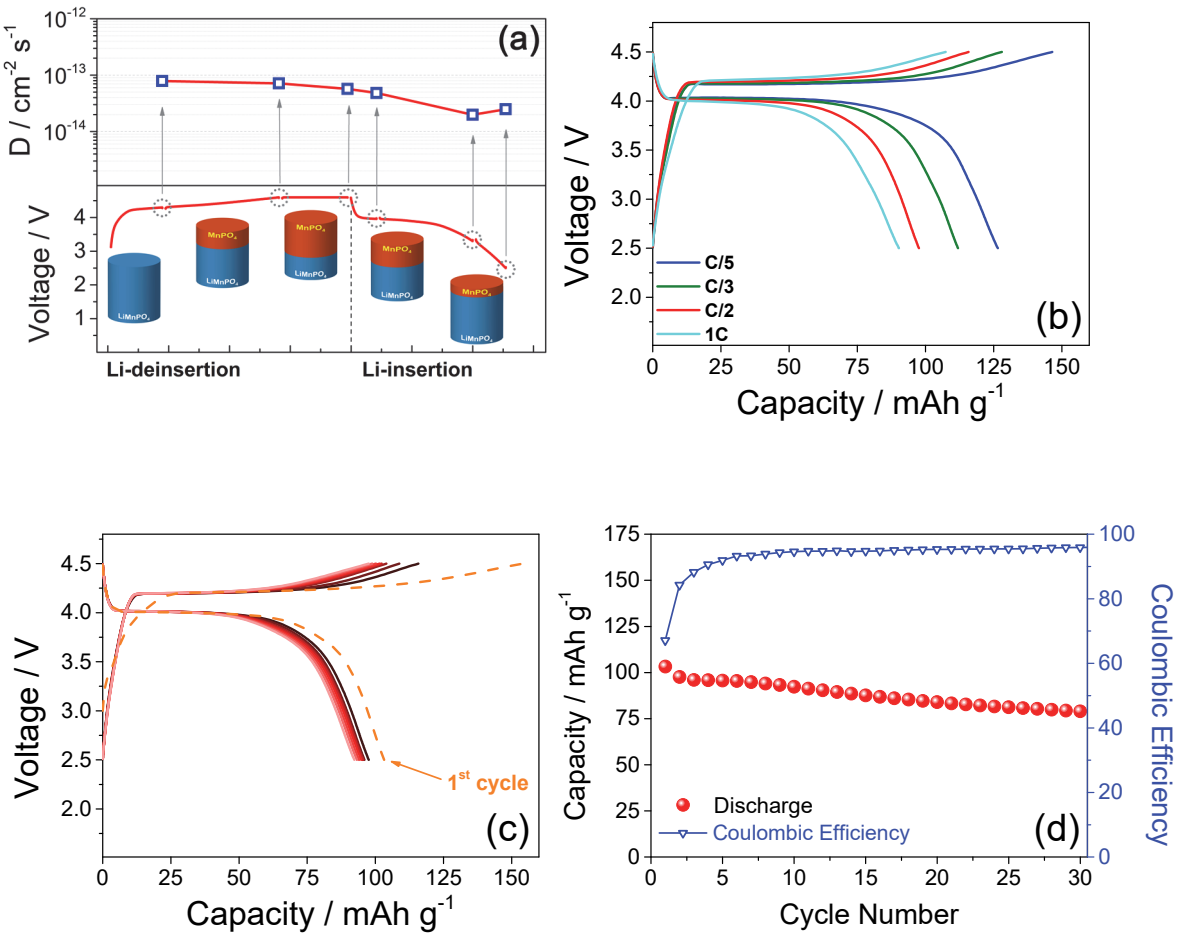

Figure 6